The Astrophysical Journal, 974:51 (9pp), 2024 October 10 https://doi.org/10.3847/1538-4357/ad712d

A Luminous X-Ray Active Galactic Nucleus in the Dwarf–Dwarf Galaxy Merger RGG 66

Seth J. Kimbrell[1,2] and Amy E. Reines[2]
[1] Department of Physics and Astronomy, Carleton College, MN 55057, USA; skimbrell@carleton.edu
[2] eXtreme Gravity Institute, Department of Physics, Montana State University, MT 59715, USA
Received 2024 February 14; revised 2024 August 8; accepted 2024 August 16; published 2024 October 4

Abstract

We present the discovery of a luminous X-ray active galactic nucleus (AGN) in the dwarf galaxy merger RGG 66. The black hole is predicted to have a mass of $M_{\rm BH} \sim 10^{5.4}\,M_{\odot}$ and to be radiating close to its Eddington limit ($L_{\rm bol}/L_{\rm Edd} \sim 0.75$). The AGN in RGG 66 is notable both for its presence in a late-stage dwarf–dwarf merger and for its luminosity of $L_{2-10\,\rm keV} = 10^{42.2}$ erg s^{-1}, which is among the most powerful AGNs known in nearby dwarf galaxies. The X-ray spectrum has a best-fit photon index of $\Gamma = 2.4$ and an intrinsic absorption of $N_H \sim 10^{21}$ cm^{-2}. These results come from a follow-up Chandra X-ray Observatory study of four irregular/disturbed dwarf galaxies with evidence for hosting AGNs based on optical spectroscopy. The remaining three dwarf galaxies do not have detectable X-ray sources with upper limits of $L_{2-10\,\rm keV} \lesssim 10^{40}$ erg s^{-1}. Taken at face value, our results on RGG 66 suggest that mergers may trigger the most luminous of AGNs in the dwarf galaxy regime, just as they are suspected to do in more massive galaxy mergers.

Unified Astronomy Thesaurus concepts: AGN host galaxies (2017); X-ray active galactic nuclei (2035); Dwarf galaxies (416); Galaxy mergers (608)

1. Introduction

In recent years, massive black holes (BHs) in dwarf galaxies ($M_{\rm BH} \sim 10^4 - 10^6\,M_{\odot}$) have been increasingly discovered and studied in detail (for a review, see A. E. Reines 2022). These systems provide clues to BH seeding as they give us an opportunity to study BHs that have not grown much compared to the supermassive BHs ($M_{\rm BH} \sim 10^6 - 10^9\,M_{\odot}$), which are ubiquitous in more massive galaxies. At the same time, studying the demographics and morphologies of the dwarf galaxy hosts gives us a chance to characterize the environments inhabited by these BHs. Moreover, since current capabilities do not allow us to directly observe the first seed BHs in the early Universe, nearby dwarf galaxies hosting the smallest BHs offer our best chance put constraints on possible formation channels (M. Volonteri 2010; J. E. Greene et al. 2020; K. Inayoshi et al. 2020; M. Volonteri et al. 2021).

Additionally, dwarf galaxy mergers are expected to be common in the earlier Universe, and they have been shown to trigger periods of intense star formation in the present-day Universe, leading to the formation of blue compact dwarf (BCD) galaxies (S. Stierwalt et al. 2015; S. Paudel et al. 2018). However, active BHs in dwarf–dwarf mergers are an understudied area. The quintessential AGN in a dwarf–dwarf merger is Mrk 709 (A. E. Reines et al. 2014; E. Kimbro et al. 2021), a system in which an AGN has been detected in one of the members of an early-stage merger. M. Mićić et al. (2023) reported the discovery of strong candidates for the first dual AGNs in dwarf–dwarf mergers; systems in which the separation between the two AGNs are great enough to be resolvable (on the scale of kiloparsecs).

Here we present Chandra X-ray Observatory observations of four irregular/disturbed dwarf galaxies. Our sample comes from the work of S. J. Kimbrell et al. (2021), who used Hubble Space Telescope (HST) observations to study the structures and morphologies of dwarf galaxies that were selected by A. E. Reines et al. (2013) as strong candidates for hosting active massive BHs based on optical spectroscopy from the Sloan Digital Sky Survey (SDSS).

The primary focus of this work is the detection of a luminous X-ray AGN in the late-stage dwarf–dwarf merger, RGG 66 (ID 66 in the A. E. Reines et al. 2013 paper). In Section 2, we describe our sample of dwarf galaxies in more detail. In Section 3, we describe the X-ray observations. We present our analysis and results for RGG 66 in Section 4 and discuss the targets with nondetections in Section 5. We finish with our conclusions in Section 6.

2. Sample of Dwarf Galaxies

Our sample of disturbed/irregular dwarf galaxies comes from S. J. Kimbrell et al. (2021). In that work, S. J. Kimbrell et al. (2021) analyzed HST near-IR imaging of a subsample of 41 dwarf galaxies that were identified by A. E. Reines et al. (2013) as likely AGN hosts based on narrow emission-line ratio diagnostics (L. J. Kewley et al. 2006; G. Kauffmann et al. 2003; L. J. Kewley et al. 2001). Six of the dwarf galaxies were classified as "irregular/disturbed," broadly indicating that the galaxy could not be modeled by axisymmetric models. Of those six, three appeared to be Magellanic-type dwarf irregulars, while two exhibited clear signatures of interactions or mergers. The final galaxy possessed internal spiral structure that made modeling difficult, but it did not fall into either the Magellanic-type irregular or disturbed category.

We excluded the galaxy with an internal spiral (RGG 53), as well as one of the Magellanic-type irregulars (RGG 5), which had previously been observed by Chandra with no X-ray source detected. Of the four remaining galaxies (see Figure 1), two are Magellanic-type irregular dwarf galaxies (RGG 40 and RGG 136), and two show signs of interactions/mergers (RGG 66 and RGG 135). All four of these dwarf galaxies were identified as Seyferts in the [O III]/Hβ versus [S II]/Hα diagnostic, and all fell into the composite region of the [O III]/Hβ versus [N II]/Hα diagnostic (Figure 2). We observed these four galaxies with Chandra, and the galaxy properties are shown in

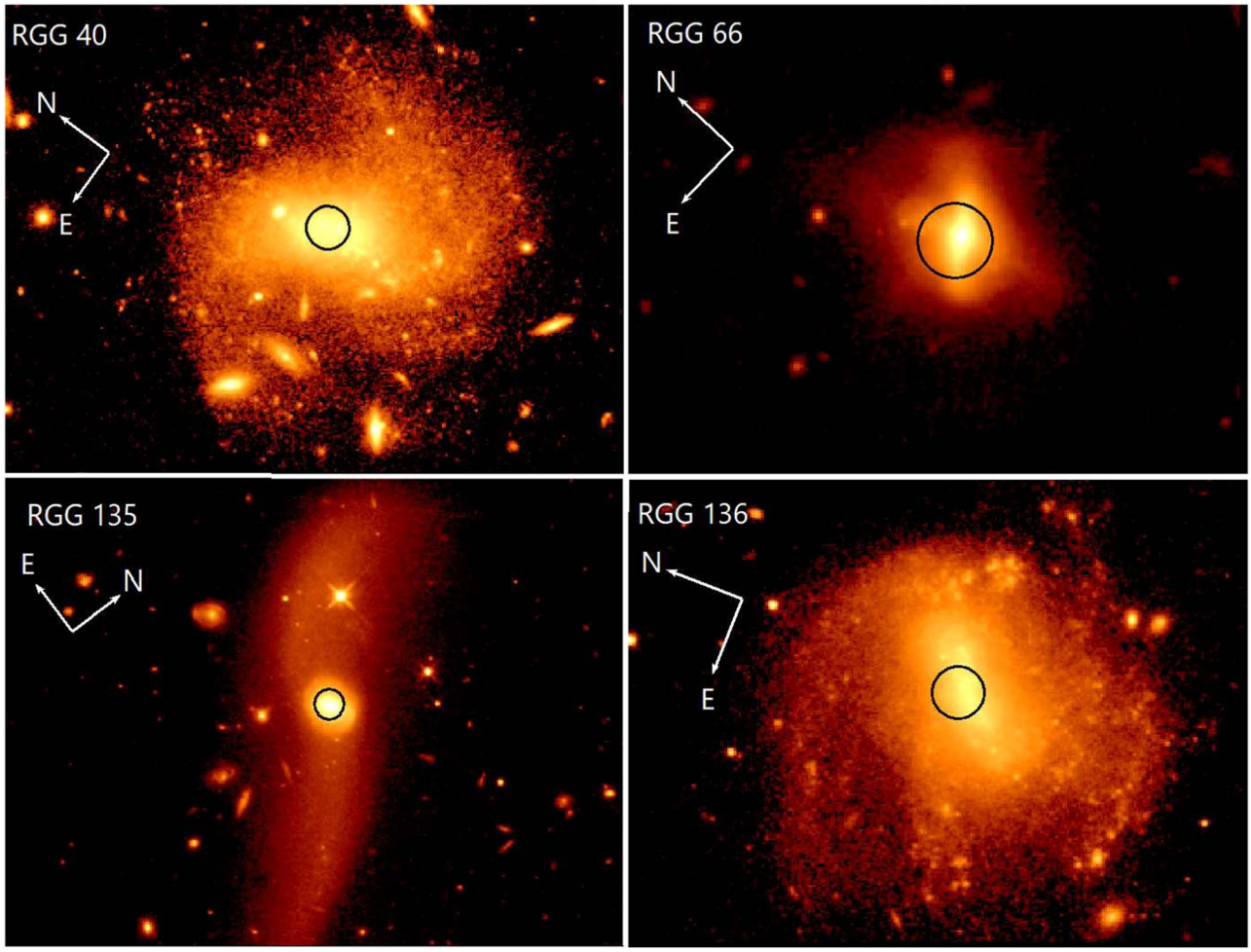

Figure 1. Near-IR observations from HST (S. J. Kimbrell et al. 2021) of the four dwarf irregular galaxies analyzed in this work. The black circle indicates the 3″ diameter SDSS spectroscopic fiber, with fiber positions obtained from the NSA.

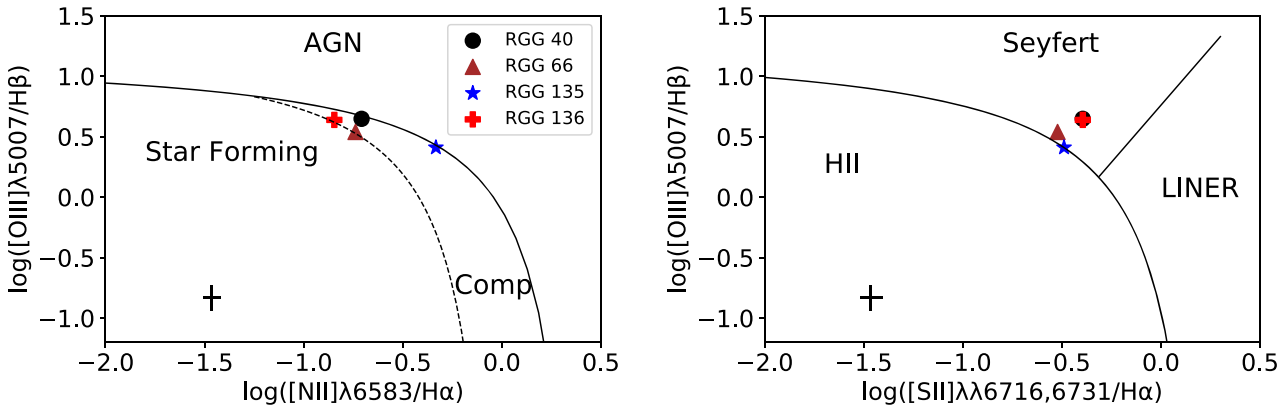

Figure 2. Narrow emission-line diagnostic diagrams for our sample of irregular dwarf galaxies, which were identified as displaying optical signatures of active massive BHs by A. E. Reines et al. (2013), and which were analyzed by S. J. Kimbrell et al. (2021). Left: [O III]/Hβ vs. [N II]/Hα diagnostic diagram, with the "maximum starburst" line from stellar photoionization models (L. J. Kewley et al. 2001) shown as the solid line, and the empirical separation from G. Kauffmann et al. (2003) between galaxies whose emission is dominated by star formation and galaxies with some contribution from AGN shown as the dashed line. Right: [O III]/Hβ vs. [S II]/Hα diagnostic diagram, adopting the classifications from L. J. Kewley et al. (2006). Typical errors are shown in the lower left corners.

Table 1. Distances are obtained from the NASA Sloan Atlas (NSA), assuming $h = 0.73$. Galactic neutral hydrogen column densities come from J. M. Dickey & F. J. Lockman (1990) and are retrieved from Chandra's Colden Galactic Neutral Hydrogen Density Calculator.[3]

[3] https://cxc.harvard.edu/toolkit/colden.jsp

3. Chandra X-Ray Observations

Our target galaxies were observed by Chandra between 2021 November 12 and 2023 January 19 with exposure times ranging from 9 to 35 ks (Table 1). For each observation, the target galaxy was centered on the ACIS S3 chip.

Using version 4.14 of the Chandra Interactive Analysis of Observations (CIAO) software (A. Fruscione et al. 2006), we

Table 1
Irregular/Disturbed Dwarf Galaxy Sample

RGG ID	NSA ID	Obs. ID	R.A. (deg)	Decl. (deg)	z	r_{50} (kpc)	log $(M_*/M_\odot)$	N_H (10^{20} cm^{-2})	Observation Time (ks)
(1)	(2)	(3)	(4)	(5)	(6)	(7)	(8)	(9)	(10)
RGG 40	82616	25280	117.12165	51.01453	0.0190	3.91	9.1	5.14	8.96
RGG 66	55081	25281, 26315	154.44624	39.53551	0.0540	0.40	9.0	1.39	34.87[a]
RGG 135	4308	25282	263.01240	59.98194	0.0291	3.06	9.4	3.46	19.79
RGG 136	5563	25283	359.03827	−0.40800	0.0256	5.32	9.2	3.40	15.87

Note. Column (1): ID given in A. E. Reines et al. (2013) and S. J. Kimbrell et al. (2021). Column (2): NSA identification number. Column (3): Chandra observation ID. Column (4): R.A. of the galaxy. Column (5): decl. of the galaxy. Column (6): redshift taken from the NSA. Column (7): Petrosian 50% light radius, from the NSA. Column (8): log total stellar mass from the NSA. Column (9): galactic neutral hydrogen column density. Column (10): exposure time in kiloseconds.
[a] RGG 66 was observed twice—one observation of 18.79 ks and one of 16.08 ks, and we merged the observations for analysis.

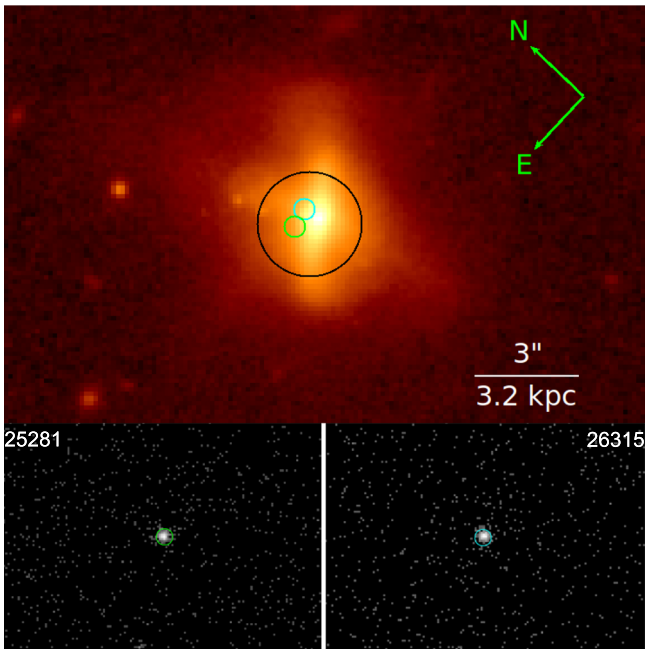

Figure 3. Top: near-infrared (F110W) HST image of RGG 66 shown on a log scale. The black circle shows the position of the SDSS spectroscopic fiber, while the smaller green and cyan circles show the position and positional uncertainty of the detected X-ray source for observations 25281 and 26315, respectively. The different positions of the X-ray source from the two observations is due to the pointing accuracy of Chandra rather than a real offset. Bottom: Chandra images for observations 25281 and 26315, with source apertures shown following the same color pattern as above.

first reprocessed our data utilizing the chandra_repro script. We applied Chandra calibration files (CALDB 4.9.8) for reprocessing, filtered for any background flares, and created new event files, which were used in our analysis.

We then attempted to correct the absolute astrometry of our images using the SDSS. We ran the CIAO wavdetect routine[4] on each filtered image using wavelets of size 1.0, 1.4, 2.0, 2.8, and 4.0 pixels. We set our significance threshold to be 10^{-6}; this is the threshold at which we should expect roughly one strong background fluctuation to be detected as a source across the entire chip. If any X-ray sources were found outside the target galaxies, we matched them to existing SDSS detections. However, no matching sources were located for our images, and so astrometry corrections could not be performed in the end.

Next, we searched for X-ray point sources that could correspond to active massive BHs in our target galaxies. We began by filtering our images from 2 to 7 keV and running wavdetect. For our point-spread function (PSF) map, we created a PSF map using the CIAO fluximage routine with an enclosed energy fraction of 39% at 4 keV. Once wavdetect identified point sources, we filtered by location in the image and only accepted X-ray sources that are within $3r_{50}$ of the center of the galaxy. We detect an X-ray source in one of our four target galaxies, RGG 66. We show the location of the X-ray source in RGG 66 along with the SDSS fiber position in the top panel of Figure 3.

For the other three galaxies, in which no sources were found by wavdetect, we determine upper limits on the fluxes/luminosities of potential X-ray sources at the 95% confidence level via Poisson statistics using srcflux.[5] We center a 4″ radius circular source region at the aimpoint of the image, and we extract background counts using an annulus centered at the aimpoint of the image, with inner radius 4″ and outer radius 20″. We assume an absorbed power-law spectral model using the Galactic N_H values toward each galaxy and a photon index of $\Gamma = 1.8$, a typical value for low-luminosity AGN (L. J. Latimer et al. 2021; L. C. Ho 2009, 2008). We find upper limits on the hard X-ray luminosities of $L_{2-10\,\mathrm{keV}} \lesssim 10^{40}\,\mathrm{erg\,s^{-1}}$ for the three galaxies with nondetections (see Table 3).

4. A Luminous X-Ray AGN in RGG 66

4.1. X-Ray Source Properties

We detected a bright X-ray source in each of the two observations of RGG 66 using wavdetect. The source is offset by ∼0.″65 (∼1.3 pixels) in the two observations. Given that the offset is within the absolute astrometric uncertainties of Chandra (∼1″) and the count rates are the same (see below), we conclude that we are detecting the same source in the two images.

The positions and positional uncertainties in each image are given in Table 2. The positional uncertainty is given as the 95% error circle in the wavedetect source position using the relation from J. Hong et al. (2005), which depends on the offset from the aimpoint, D (in arcminutes), and the net counts, c_n:

$$P_{\mathrm{err}} = 0.''25 + \frac{0.''1}{\log(c_n+1)}\left[1+\frac{1}{\log(c_n+1)}\right] + 0.''03\left[\frac{D}{\log(c_n+2)}\right]^2 + 0.''0006\left[\frac{D}{\log(c_n+3)}\right]^4. \quad (1)$$

[4] https://cxc.cfa.harvard.edu/ciao/ahelp/wavdetect.html

[5] https://cxc.cfa.harvard.edu/ciao/ahelp/srcflux.html

Table 2
RGG 66 Observations

ObsID	Source R.A. (deg)	Source Decl. (deg)	Source Pos. Error (arcsec)	Exp. Time (ks)	Net Counts (2–7 keV)	Count Rate (2–7 keV) (count s^{-1})
(1)	(2)	(3)	(4)	(5)	(6)	(7)
Detected Source						
25281	154.446325	39.535565	0.31	18.517	240.01 ± 27.43	0.0130
26315	154.446128	39.535606	0.31	16.066	209.52 ± 25.63	0.0130

Note. Column (1): observation ID. Column (2): R.A. of the X-ray source. Column (3): decl. of the X-ray source. Column (4): 95% error in position, not accounting for absolute astrometric uncertainties that are expected to be $\sim 1''$. Column (5): exposure time in kiloseconds. Column (6): net Counts from 2 to 7 keV. Column (7): count rate.

This does not account for any absolute astrometric uncertainty, which is expected to be on the order of $\sim 1''$.

To find the net counts detected in each observation, we used a circular aperture centered on each detected source with a radius enclosing 90% of the energy at 4.5 keV ($2''$). We then estimated the number of background counts by creating an annulus colocated with the source, with an inner radius equal to the radius of the source aperture and outer radius equal to 12 times the radius of the source aperture. We subtracted the background counts from the source counts to find the net counts and corrected for the 90% enclosed energy fraction.

We found net counts of 240.01 ± 27.43 (~ 0.013 counts s^{-1}) for the observation 25281 and net counts of 209.52 ± 25.63 (~ 0.013 counts s^{-1}) for observation 26315 in the 2–7 keV range. Since our source has net counts $\gg 10$, we neglected the background when calculating the errors in net counts and use the 90% confidence intervals from N. Gehrels (1986).

Given the large number of counts, we performed spectral analysis on the data for RGG 66. We used the specextract CIAO tool[6] to extract a spectrum from each observation using the same aperture and background used to find net counts, then merged the spectra using the combine_spectra CIAO tool[7] (bottom panel of Figure 3). We grouped our counts in bins of 20 then used the Sherpa fitting package to model the spectrum with an absorbed power-law model, including a Galactic absorption term $N_{H,\mathrm{gal}}$ and an intrinsic absorption term $N_{H,\mathrm{target}}$. We froze $N_{H,\mathrm{gal}}$ to the value of $1.39 \times 10^{20}\,\mathrm{cm}^{-2}$ from J. M. Dickey & F. J. Lockman (1990). We found that the spectrum was best fit by an absorbed power law with photon index $\Gamma = 2.43 \pm 0.14$ and intrinsic absorption of $N_{H,\mathrm{target}} = (9.3 \pm 6.7) \times 10^{20}\,\mathrm{cm}^{-2}$ (see Figure 4). We find an unabsorbed flux in the 2–10 keV range of $2.59 \times 10^{-13}\,\mathrm{erg\,s}^{-1}$.

The hard X-ray luminosity of the source in RGG 66 is $L_{2-10\,\mathrm{keV}} = 10^{42.18}\,\mathrm{erg\,s}^{-1}$, squarely in the AGN regime and more than $\sim 1000\times$ the expected contribution from stellar mass X-ray binaries (see Section 4.3 and Table 3).

4.2. BH Mass and Eddington Ratio

We first determine the minimum mass of the BH in RGG 66 by assuming Eddington-limited accretion. While the Eddington ratio may in fact be lower than 1, this calculation will place a lower limit on the BH mass. The Eddington luminosity is given by

$$L_{\mathrm{Edd}} \sim 1.26 \times 10^{38}\left(\frac{M_{\mathrm{BH}}}{M_{\odot}}\right), \tag{2}$$

and to determine the minimum BH mass, we assume $L_{\mathrm{Edd}} = L_{\mathrm{bol}} = \kappa L_{2-10\,\mathrm{keV}}$. We use the relation derived in F. Duras et al. (2020) to find the bolometric correction, κ, from the hard X-ray luminosity:

$$\kappa(L_x) = a\left[1 + \left(\frac{\log(L_x/L_{\odot})}{b}\right)^{c}\right], \tag{3}$$

with best-fit values of $a = 15.33 \pm 0.06$, $b = 11.48 \pm 0.01$, and $c = 16.20 \pm 0.16$. Using this relation and our measured hard X-ray luminosity, we estimate a bolometric correction of $\kappa \sim 15.47$. We then have $L_{\mathrm{Edd}} = L_{\mathrm{bol}} = \kappa L_{2-10\,\mathrm{keV}} = 2.34 \times 10^{43}\,\mathrm{erg\,s}^{-1}$, corresponding to a minimum BH mass of $M_{\mathrm{BH}} \sim 10^{5.3}\,M_{\odot}$.

Next, we estimate the BH mass using the relation in A. E. Reines & M. Volonteri (2015) between BH mass and total galaxy stellar mass for local AGNs:

$$\log(M_{\mathrm{BH}}/M_{\odot}) = \alpha + \beta \log(M_{\mathrm{stellar}}/10^{11} M_{\odot}), \tag{4}$$

with $\alpha = 7.45 \pm 0.08$ and $\beta = 1.05 \pm 0.11$. Applying this relation to RGG 66 with a total stellar mass estimate of $M_{\mathrm{stellar}} \sim 10^{9}\,M_{\odot}$ (see Table 1), we predict a BH of mass $10^{5.4}\,M_{\odot}$ with an uncertainty of ~ 0.55 dex (A. E. Reines & M. Volonteri 2015).

We can find the corresponding Eddington ratio of the BH in RGG 66 using this mass estimate and the hard X-ray luminosity of $L_{2-10\,\mathrm{keV}} = 10^{42.18}\,\mathrm{erg\,s}^{-1}$, where the Eddington ratio is given by

$$f_{\mathrm{Edd}} = \frac{\kappa \times (L_{2-10\mathrm{keV}})}{L_{\mathrm{Edd}}}. \tag{5}$$

This gives an Eddington ratio of $f_{\mathrm{Edd}} = 0.75^{+1.88}_{-0.54}$. The uncertainties come from propagating the uncertainty of 0.55 dex in the BH mass estimate using the relation from A. E. Reines & M. Volonteri (2015), which we expect to dominate the error in Eddington ratio. Our results provide evidence that RGG 66 hosts a BH with a mass of a few $\times 10^{5}\,M_{\odot}$ radiating at a high fraction of its Eddington luminosity.

[6] https://cxc.cfa.harvard.edu/ciao/ahelp/specextract.html
[7] https://cxc.cfa.harvard.edu/ciao/ahelp/combine_spectra.html

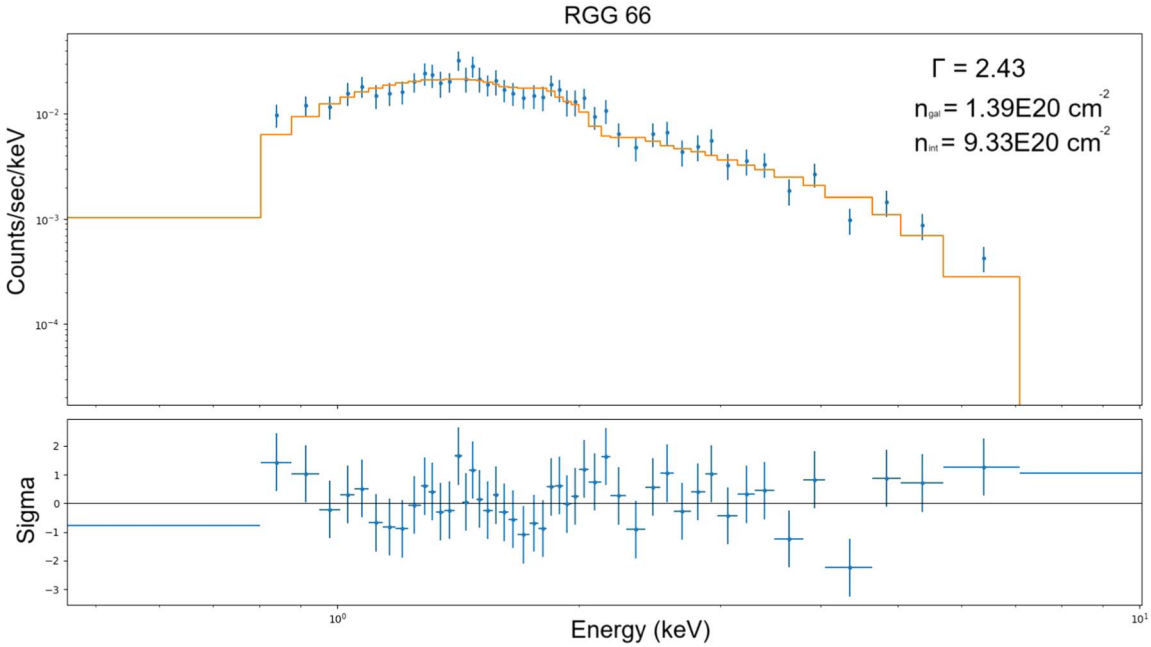

Figure 4. X-ray spectrum of RGG 66, with a best-fit photon index of $\Gamma = 2.43$ and counts grouped in bins of 20.

Table 3
X-Ray Sources

Name	R.A.	Decl.	Net Counts		Flux (10^{-15} erg s^{-1} cm^{-2})		Luminosity (log(erg s^{-1}))	
	(deg)	(deg)	0.5–2 keV	2–7 keV	0.5–2 keV	2–10 keV	0.5–2 keV	2–10 keV
(1)	(2)	(3)	(4)	(5)	(6)	(7)	(8)	(9)
Detected Source								
RGG 66	154.446334	39.535563	853.73 ± 51.24	465.01 ± 36.00	436.08	259.08	42.42	42.18
Upper Limits on Nondetections								
RGG 40	⋯	⋯	⋯	⋯	<4.71	<11.0	<39.54	<39.90
RGG 135	⋯	⋯	⋯	⋯	<4.84	<12.3	<39.92	<40.32
RGG 136	⋯	⋯	⋯	⋯	<3.59	<8.56	<39.68	<40.05

Note. Column (1): galaxy ID. Column (2): R.A. of the X-ray source, identified by wavdetect. Column (3): decl. of the X-ray source, identified by wavdetect. Columns (4)–(5): aperture-corrected net counts from the combined spectrum. Columns (6)–(7): absorption-corrected flux. Columns (8)–(9): absorption-corrected log luminosity.

4.3. Host Galaxy

We first examine the properties of RGG 66 using the NSA to confirm its classification as a dwarf galaxy system. To begin, its Petrosian 50% light radius of $r_{50} = 0.4$ kpc speaks to a compact system. We also compare the absolute magnitudes of RGG 66 and compare them to those found in literature for known dwarf galaxies. The AGN-hosting dwarf–dwarf merger system Mrk 709 (A. E. Reines et al. 2014; E. Kimbro et al. 2021) has absolute g-, r-, and i- band magnitudes of ~ -20. For comparison, RGG 66 has absolute magnitudes of ~ -18.2, -18.7, and -18.5 in the g, r, and i bands. The g-band magnitude of RGG 66 is comparable with the rest of the A. E. Reines et al. (2013) sample of dwarf galaxies from which it was drawn. These parameters, along with its stellar mass estimate of $M_\star \sim 10^9 M_\odot$, allow us to confidently describe RGG 66 as a dwarf.

We use visual inspection of RGG 66 in classifying it as a merger. The HST image (top panel of Figure 3) shows tidal features running left to right in the image. These tidal tails are indicators of a galaxy merger/interaction. The presence of these features without a companion galaxy in the vicinity leads us to classify RGG 66 as a late-stage merger near the point of coalescence.

We estimate the star formation rate of RGG 66 using far-UV and mid-IR luminosity measurements from the Galaxy Evolution Explorer (GALEX) All-Sky Catalog and the Wide-field Infrared Explorer (WISE):

$$L(\mathrm{FUV})_{\mathrm{corr}} = L(\mathrm{FUV})_{\mathrm{obs}} + 3.89L(25\ \mu\mathrm{m}) \quad (6)$$

$$\log \dot{M}(M_\odot \mathrm{yr}^{-1}) = \log L(\mathrm{FUV}_{\mathrm{corr}}) - 43.35 \quad (7)$$

(C.-N. Hao et al. 2011; R. C. Kennicutt & N. J. Evans 2012). The GALEX FUV luminosity is obtained via measurements in the NSA. While the calibrations above utilized 25 μm luminosities from the Infrared Astronomical Satellite, we use 22 μm observations from WISE as the flux density ratio at these wavelengths is of order unity (T. H. Jarrett et al. 2013).

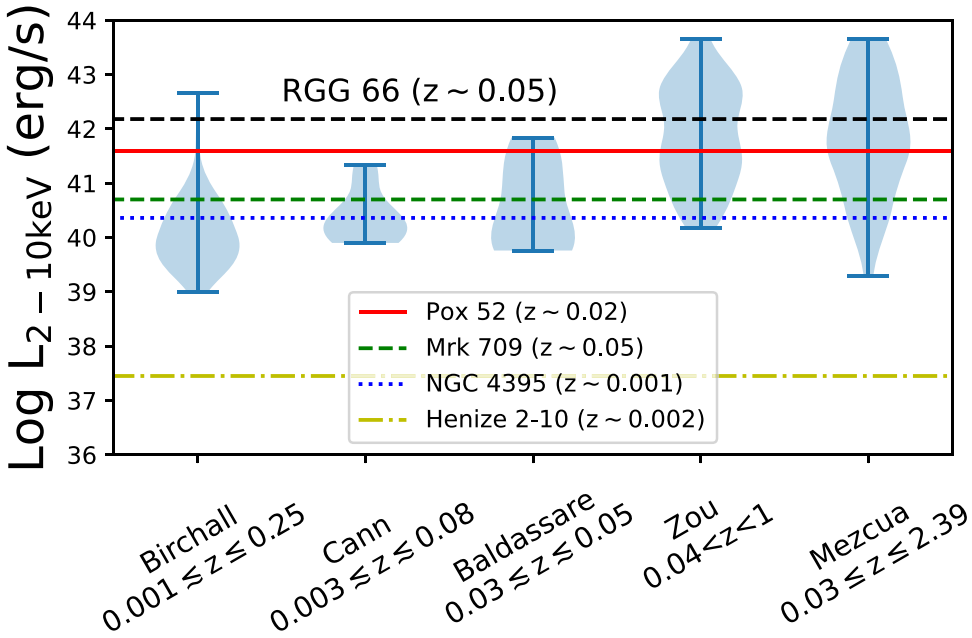

Figure 5. X-ray luminosities in the 2–10 keV band of the source in RGG 66 compared to the sources studied in J. M. Cann et al. (2024), F. Zou et al. (2023), K. L. Birchall et al. (2020), M. Mezcua et al. (2018), and V. F. Baldassare et al. (2017), as well as Pox 52 and NGC 4395 (G. C. Dewangan et al. 2008), along with Mrk 709 (A. E. Reines et al. 2014) and Henize 2–10 (A. E. Reines et al. 2016). The range of luminosities for each sample is shown using the blue lines, while the width of the blue shaded region denotes the fraction of the sample at that luminosity. Luminosities have been transformed to the 2–10 keV range where necessary (see Section 4.4).

For RGG 66, with $\log L(\mathrm{FUV})[\mathrm{erg\,s^{-1}}] = 42.48$ and $\log L(22\ \mu\mathrm{m})[\mathrm{erg\,s^{-1}}] = 42.08$, we expect a star formation rate (SFR) of $0.34\,M_{\odot}\,\mathrm{yr^{-1}}$ (assuming the mid-IR and FUV luminosities are dominated by star formation and any contribution from the AGN is negligible).

The corresponding specific star formation rate is $3.45 \times 10^{-10}\,\mathrm{yr^{-1}}$. At this specific star formation rate, we expect to see a contribution to the galaxy-wide X-ray luminosity from high-mass X-ray binaries (HMXB), which scale with star formation rate, with additional contributions from low-mass X-ray binaries (LMXB), which scale with galaxy mass (H.-J. Grimm et al. 2003; E. J. M. Colbert et al. 2004; B. D. Lehmer et al. 2010; S. Mineo et al. 2012).

We use the following relation from B. D. Lehmer et al. (2010) to estimate the contribution from both HMXBs and LMXBs:

$$L_{\mathrm{HX}}^{\mathrm{gal}} = \alpha M_{*} + \beta \mathrm{SFR}, \tag{8}$$

where $\alpha = (9.05 \pm 0.37) \times 10^{28}\,\mathrm{erg\,s^{-1}} M_{\odot}^{-1}$ and $\beta = (1.62 \pm 0.22) \times 10^{39}\,\mathrm{erg\,s^{-1}} (M_{\odot}\,\mathrm{yr^{-1}})^{-1}$ (with a 1σ scatter of 0.34 dex). For RGG 66, the expected 2–10 keV luminosity from X-ray binaries is $\sim 10^{38.8}\,\mathrm{erg\,s^{-1}}$. This is more than 3 orders of magnitude below the measured hard X-ray luminosity, indicating that the X-ray source in RGG 66 is due to an AGN.

The AGN in RGG 66 is also detected at radio wavelengths by the Very Large Array Sky Survey (VLASS). Eberhard et al. (2024) present a search for radio AGNs in dwarf galaxies using VLASS and identify this object in their sample (ID 4 in that work). The radio source has a luminosity of $L_{3\mathrm{GHz}} = 10^{21.9}\,\mathrm{W\,Hz^{-1}}$.

4.4. Comparison to Other AGNs in Dwarf Galaxies

We compare the X-ray luminosity of the active BH in RGG 66 to other low-mass AGNs in dwarf galaxies. Using the spectrum of RGG 66, we find a broadband X-ray luminosity of $\log(L_{0.5-8\mathrm{keV}}) = 42.18$, significantly higher than the majority of known AGNs in nearby dwarf galaxies with X-ray observations (Figure 5).

Two of the most well-studied dwarf galaxies hosting optically selected AGNs are NGC 4395 (A. V. Filippenko & L. C. Ho 2003) and Pox 52 (A. J. Barth et al. 2004). While NGC 4395 is variable in the X-ray (P. Lira et al. 1999; E. C. Moran et al. 2005), measurements of its hard X-ray luminosity have generally been found to be on the order of $L_{2-10\,\mathrm{keV}} \sim 10^{40}\,\mathrm{erg\,s^{-1}}$ (E. C. Moran et al. 2005; S. Vaughan et al. 2005; G. C. Dewangan et al. 2008). Pox 52 was found by G. C. Dewangan et al. (2008) to have a 2–10 keV luminosity of $\sim 10^{41.61}$ using XMM-Newton observations. The nearby ($d \sim 9$ Mpc) dwarf starburst galaxy Henize 2–10 also hosts a massive BH at its center. This was observed using Chandra by A. E. Reines et al. (2016) and found to have a 0.3–10 keV luminosity $\sim 10^{38}\,\mathrm{erg\,s^{-1}}$. Another massive BH resides in the dwarf galaxy pair Mrk 709 (A. E. Reines et al. 2014), which was observed by Chandra in that work and found to have a 2–10 keV luminosity of $10^{40.7}\,\mathrm{erg\,s^{-1}}$.

A number of studies have also focused on the X-ray properties of larger samples of AGNs in dwarf galaxies. For example, the ten broad-line AGNs in the A. E. Reines et al. (2013) sample of dwarf galaxies with optical AGN signatures have 2–10 keV X-ray luminosities in the range $L_{2-10\,\mathrm{keV}} = 10^{39.8}$ to $10^{41.8}\,\mathrm{erg\,s^{-1}}$ (V. F. Baldassare et al. 2017).

L. J. Latimer et al. (2019) performed a combined X-ray and radio search among BCD galaxies and located one candidate AGN in Haro 9. That AGN candidate had a 2–10 keV luminosity of $L_{2-10\,\mathrm{keV}} = 10^{39.4}\,\mathrm{erg\,s^{-1}}$. In a later work, L. J. Latimer et al. (2021) performed an X-ray study of WISE-selected AGN candidates in dwarf galaxies. The five galaxies that they identified as having strong evidence for an accreting central BH had hard X-ray luminosities in the range $10^{40.1}-10^{41.9}\,\mathrm{erg\,s^{-1}}$, with a median of $10^{40.3}\,\mathrm{erg\,s^{-1}}$.

K. L. Birchall et al. (2020) presented a study of 61 X-ray selected AGNs in nearby ($z \leqslant 0.25$) dwarf galaxies with X-ray

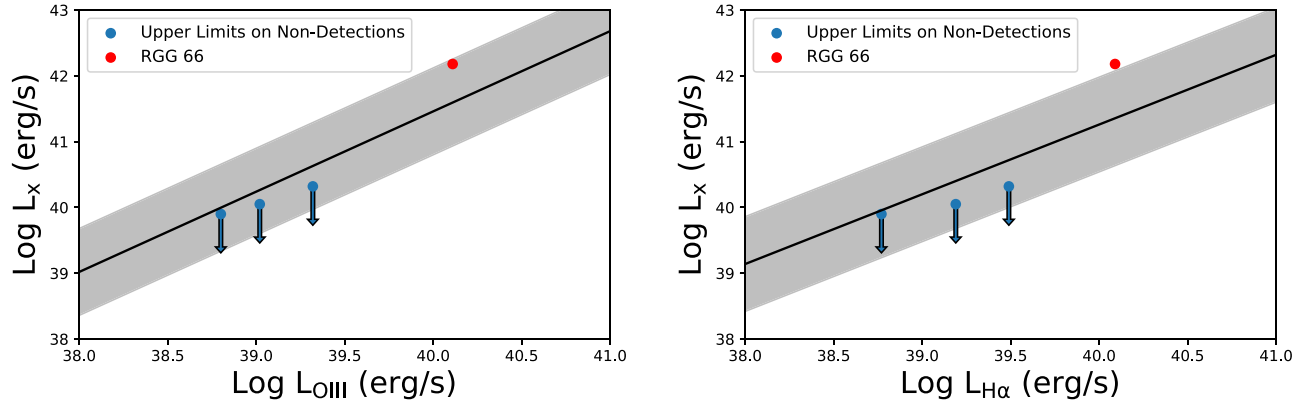

Figure 6. Observed and upper limit 2–10 keV luminosity vs observed O III luminosity (top) and H_α luminosity (bottom) in ergs per second. The black line shows the F. Panessa et al. (2006) relation, and the gray shading shows the scatter derived in L. J. Latimer et al. (2021).

luminosities given in the 2–12 keV band. RGG 66 has an X-ray luminosity of $10^{42.18}$ erg s^{-1}, which is at the very high end of the range measured there. K. L. Birchall et al. (2020) found 2–12 keV X-ray luminosities between $10^{39.05}$ erg s^{-1} and $10^{42.73}$ erg s^{-1}, with a median of $10^{40.04}$ erg s^{-1} (see Figure 4 of that work). In fact, RGG 66 has a higher hard X-ray luminosity than all but one dwarf galaxy reported in Table B1 of that work.

F. Zou et al. (2023) searched for active dwarf galaxies in the XMM-Spitzer Extragalactic Representative Volume Survey. In that work, 73 active dwarf galaxies with redshift $z \leqslant 1$ had their X-ray properties measured; X-ray luminosities in the 2–10 keV band ranged from $10^{40.18}$ to $10^{43.66}$ erg s^{-1}, with a median of $10^{41.85}$ erg s^{-1} and a mean of $10^{41.86}$ erg s^{-1}.

J. M. Cann et al. (2024) explored archival XMM observations of 37 low-metallicity dwarf galaxies and examined their X-ray properties. In that work, ten galaxies were defined as candidate AGN hosts using the criterion that the X-ray luminosity in the 0.3–10 keV range exceeded 10^{40} erg s^{-1}. These ten had full-band X-ray luminosities ranging from $10^{40.13}$ to $10^{41.56}$ erg s^{-1}.

M. Mezcua et al. (2018) searched the Chandra COSMOS-Legacy survey and found 40 dwarf galaxies hosting AGNs at redshifts as far out as $z \sim 2.4$. In that work, X-ray luminosities were reported in the 0.5–10 keV range and fell in the range of $10^{39.5}$–$10^{43.9}$ erg s^{-1}, with a median of 10^{42} erg s^{-1} and a mean of $10^{42.08}$ erg s^{-1}. Similar to RGG 66 in this work, many of the AGNs studied in M. Mezcua et al. (2018) are accreting at very high Eddington ratios.

The massive BH in RGG 66 shares similarities with those found in M. Mićić et al. (2023). In that work, two dwarf–dwarf merger systems with redshifts ∼0.27 were identified as candidate dual AGNs (i.e., AGNs resolvable as two separate sources). In particular, the AGNs with pair separations of <5 kpc in the galaxies named Elstir and Vinteuil have broadband luminosities of $\log(L_{0.5-8\mathrm{keV}}) = 41.96$ and 42.71 in erg s^{-1}, which are similar to that of the AGN in RGG 66. Unlike RGG 66, which appears to be a system at the coalescence stage of the merger, Elstir and Vinteuil appear to be in the very early stages of merging.

In a follow-up work, M. Mićić et al. (2024) used HST and Chandra imaging to identify six more AGNs in dwarf–dwarf mergers. The AGNs presented in that work have luminosities in the 0.3–7 keV band ranging from $10^{40.06}$ to $10^{43.56}$ erg s^{-1}. Five of the six systems have $\log(L) < 10^{42}$ erg s^{-1}, and the remaining source is an outlier, with $\log(L) = 10^{43.56}$ erg s^{-1}.

Figure 5 shows the 2–10 keV luminosities of the aforementioned BHs along with RGG 66. Luminosities that were not reported in the 2–10 keV energy band were converted from their reported energy band using the Portable, Interactive Multi-Mission Simulator.[8] We assumed a photon index of $\Gamma = 1.8$ and $N_H = N_{H,\mathrm{GAL}}$. Some of the above BHs had spectral analysis performed or had fluxes obtained from a catalog that assumed values of Γ and/or N_H; in this case, we used the values used in the work. The X-ray source in RGG 66 has a higher luminosity than any other comparably local source discussed above. While RGG 66 lies at $z = 0.054$, the next closest object with a 2–10 keV luminosity $\geqslant 10^{42.18}$ is in the F. Zou et al. (2023) sample and lies at a redshift of 0.22.

5. Targets with Nondetections

The three galaxies without X-ray detections have upper limits on their 2–10 keV luminosities of $L_{2-10\,\mathrm{keV}} \lesssim 10^{40}$ erg s^{-1} (Section 3). Here we compare these upper limits to expectations based on multiwavelength AGN scaling relations for more massive galaxies. In particular, we compare our results to the relationships between L_X, $L_{\mathrm{H}\alpha}$, and $L_{\mathrm{O\,III}}$ from F. Panessa et al. (2006):

$$\log(L_X) = (1.06 \pm 0.04)\log(L_{\mathrm{H}\alpha}) + (-1.14 \pm 1.78), \quad (9)$$

$$\log(L_X) = (1.22 \pm 0.06)\log(L_{[\mathrm{OIII}]}) + (-7.34 \pm 2.53), \quad (10)$$

where the luminosities are in erg s^{-1}. These relations come from a sample of 47 Seyfert galaxies in the Palomar optical spectroscopic survey of nearby galaxies (L. C. Ho et al. 1997). L. J. Latimer et al. (2021) estimated the scatter in the F. Panessa et al. (2006) relations and found ∼0.72 dex for the L_X–$L_{\mathrm{H}\alpha}$ relation and a scatter of ∼0.66 dex for the L_X–$L_{\mathrm{O\,III}}$ relation.

We obtain [O III] and Hα luminosities from A. E. Reines et al. (2013) and use these to predict 2–10 keV luminosities. Figure 6 shows that the upper limits fall within the scatter of both relations and the nondetections do not rule out the presence of low-luminosity AGNs given their optical line strengths. Moreover, there is a growing body of evidence that AGNs in dwarf galaxies tend to be less bright in X-rays than expected from typical scaling relations derived from more massive galaxies hosting AGNs, with possible explanations for the low X-ray luminosities including obscuration and intrinsic

[8] https://cxc.harvard.edu/toolkit/pimms.jsp

X-ray weakness (e.g., L. J. Latimer et al. 2021; R. Arcodia et al. 2024). In any case, it is quite possible that RGG 40, RGG 135, and RGG 136, which all have optical line ratios supporting the case for AGNs, host AGNs with low enough X-ray luminosities to be undetected by this search.

6. Conclusions

We have presented Chandra observations of four low-mass irregular dwarf galaxies that were optically selected (via narrow-line diagnostic diagrams) as hosts of active massive BHs (A. E. Reines et al. 2013; S. J. Kimbrell et al. 2021). We have detected a luminous AGN in the late-stage dwarf–dwarf merger RGG 66. This is one of the first AGNs detected in such a late-stage merger of dwarf galaxies. A summary of our results is given below.

1. The X-ray source detected in RGG 66 is almost certainly an AGN, as the observed hard X-ray luminosity of $L_{20-10\,\mathrm{keV}} = 10^{42.18}\,\mathrm{erg\,s^{-1}}$ is nearly 3 orders of magnitude higher than that expected from X-ray binaries given the host galaxy star formation rate and stellar mass.
2. The corresponding minimum BH mass estimated assuming Eddington-limit accretion is $M_{\mathrm{BH}} = 10^{5.3}\,M_{\odot}$. Using the BH mass–total stellar mass relation of A. E. Reines & M. Volonteri (2015), we predict a BH of mass $M_{\mathrm{BH}} \sim 10^{5.4}\,M_{\odot}$. The corresponding Eddington ratio is $f_{\mathrm{Edd}} \sim 0.75$. These results indicate that the BH has a mass of a few hundred thousand solar masses and is radiating close to its Eddington limit.
3. The X-ray spectrum of the AGN in RGG 66 is best fit by an absorbed power-law model with a photon index of $\Gamma = 2.43 \pm 0.14$ and intrinsic absorption of $N_{H,\mathrm{target}} = (9.3 \pm 6.7) \times 10^{20}\,\mathrm{cm^{-2}}$.
4. The remaining three irregular/disturbed dwarf galaxies with optically selected AGNs in our sample are not detected in X-rays with upper limits of $L_{2-10\,\mathrm{keV}} \lesssim 10^{40}\,\mathrm{erg\,s^{-1}}$. While X-ray detections would have helped confirm the presence of accreting massive BHs in these galaxies, the lack of detectable X-ray emission does not rule out the presence of massive BHs.

The active BH in RGG 66 is also notable for being on the upper ends of the distributions of luminosity and Eddington ratio among known AGNs in dwarf galaxies. In fact, it is one of the brightest known AGNs in a dwarf galaxy at such low redshift. This may be connected to its presence in a galaxy merger, which can be conducive to efficiently fueling central massive BHs.

Indeed, simulations suggest that at least for higher-mass systems, the brightest AGNs are located in galactic mergers (P. F. Hopkins et al. 2008; P. F. Hopkins & L. Hernquist 2009). Observations suggest similar results. J. M. Comerford et al. (2015) performed an observational study of 12 dual-AGN candidates and suggested that mergers tend to host more luminous AGNs. A similar result was found by E. Treister et al. (2012), who performed a multiwavelength study of AGNs across a wide range of luminosities and redshifts and also found mergers to host the most luminous AGNs. While it is a small sample size, our results on RGG 66 taken at face value, along with results from M. Mićić et al. (2023), suggest that the trend of mergers hosting the most luminous AGNs may extend to the low-mass regime as well.

Acknowledgments

The authors thank the anonymous referee for their helpful comments and questions during the review process. The authors thank Lily Latimer for being a constant source of assistance with X-ray analysis. Support for this work was provided by NASA through Chandra Award No. GO2-23078X issued by the Chandra X-ray Observatory Center, which is operated by the Smithsonian Astrophysical Observatory for and on behalf of the NASA under contract NAS8-03060. A.E.R. also acknowledges support provided by NASA through EPSCoR grant No. 80NSSC20M0231 and the NSF through CAREER award 2235277. This work has made use of software provided by the Chandra X-ray Center (CXC) in the application packages CIAO and Sherpa. This paper employs a list of Chandra data sets, obtained by the Chandra X-ray Observatory, contained in doi:10.25574/cdc.238.

ORCID iDs

Seth J. Kimbrell https://orcid.org/0000-0003-0076-7706
Amy E. Reines https://orcid.org/0000-0001-7158-614X

References

Arcodia, R., Merloni, A., Comparat, J., et al. 2024, A&A, 681, A97
Baldassare, V. F., Reines, A. E., Gallo, E., & Greene, J. E. 2017, ApJ, 836, 20
Barth, A. J., Ho, L. C., Rutledge, R. E., & Sargent, W. L. W. 2004, ApJ, 607, 90
Birchall, K. L., Watson, M. G., & Aird, J. 2020, MNRAS, 492, 2268
Cann, J. M., Weaver, K. A., Pfeifle, R. W., et al. 2024, ApJ, 961, 178
Colbert, E. J. M., Heckman, T. M., Ptak, A. F., Strickland, D. K., & Weaver, K. A. 2004, ApJ, 602, 231
Comerford, J. M., Pooley, D., Barrows, R. S., et al. 2015, ApJ, 806, 219
Dewangan, G. C., Mathur, S., Griffiths, R. E., & Rao, A. R. 2008, ApJ, 689, 762
Dickey, J. M., & Lockman, F. J. 1990, ARA&A, 28, 215
Duras, F., Bongiorno, A., Ricci, F., et al. 2020, A&A, 636, A73
Filippenko, A. V., & Ho, L. C. 2003, ApJ, 588, 13
Eberhard, J.-M., Reines, A.E., Gim, H., Darling, J., & Greene, J.E. 2024, ApJ, submitted
Fruscione, A., McDowell, J. C., Allen, G. E., et al. 2006, Proc. SPIE, 6270, 62701V
Gehrels, N. 1986, ApJ, 303, 336
Greene, J. E., Strader, J., & Ho, L. C. 2020, ARA&A, 58, 257
Grimm, H.-J., Gilfanov, M., & Sunyaev, R. 2003, MNRAS, 339, 793
Hao, C.-N., Kennicutt, R. C., Johnson, B. D., et al. 2011, ApJ, 741, 124
Ho, L. C. 2008, ARA&A, 46, 475
Ho, L. C. 2009, ApJ, 699, 626
Ho, L. C., Filippenko, A. V., & Sargent, W. L. W. 1997, ApJS, 112, 315
Hong, J., van den Berg, M., Schlegel, E. M., et al. 2005, ApJ, 635, 907
Hopkins, P. F., & Hernquist, L. 2009, ApJ, 694, 599
Hopkins, P. F., Hernquist, L., Cox, T. J., & Kereš, D. 2008, ApJS, 175, 356
Inayoshi, K., Visbal, E., & Haiman, Z. 2020, ARA&A, 58, 27
Jarrett, T. H., Masci, F., Tsai, C. W., et al. 2013, AJ, 145, 6
Kauffmann, G., Heckman, T. M., Tremonti, C., et al. 2003, MNRAS, 346, 1055
Kennicutt, R. C., & Evans, N. J. 2012, ARA&A, 50, 531
Kewley, L. J., Dopita, M. A., Sutherland, R. S., Heisler, C. A., & Trevena, J. 2001, ApJ, 556, 121
Kewley, L. J., Groves, B., Kauffmann, G., & Heckman, T. 2006, MNRAS, 372, 961
Kimbrell, S. J., Reines, A. E., Schutte, Z., Greene, J. E., & Geha, M. 2021, ApJ, 911, 134
Kimbro, E., Reines, A. E., Molina, M., Deller, A. T., & Stern, D. 2021, ApJ, 912, 89
Latimer, L. J., Reines, A. E., Hainline, K. N., Greene, J. E., & Stern, D. 2021, ApJ, 914, 133
Latimer, L. J., Reines, A. E., Plotkin, R. M., Russell, T. D., & Condon, J. J. 2019, ApJ, 884, 78
Lehmer, B. D., Alexander, D. M., Bauer, F. E., et al. 2010, ApJ, 724, 559
Lira, P., Lawrence, A., O'Brien, P., et al. 1999, MNRAS, 305, 109
Mezcua, M., Civano, F., Marchesi, S., et al. 2018, MNRAS, 478, 2576

Mićić, M., Holmes, O. J., Wells, B. N., & Irwin, J. A. 2023, ApJ, 944, 160
Mićić, M., Irwin, J. A., Nair, P., et al. 2024, ApJL, 968, L21
Mineo, S., Gilfanov, M., & Sunyaev, R. 2012, MNRAS, 419, 2095
Moran, E. C., Eracleous, M., Leighly, K. M., et al. 2005, AJ, 129, 2108
Panessa, F., Bassani, L., Cappi, M., et al. 2006, A&A, 455, 173
Paudel, S., Smith, R., Yoon, S. J., Calderón-Castillo, P., & Duc, P.-A. 2018, ApJS, 237, 36
Reines, A. E. 2022, NatAs, 6, 26
Reines, A. E., Greene, J. E., & Geha, M. 2013, ApJ, 775, 116
Reines, A. E., Plotkin, R. M., Russell, T. D., et al. 2014, ApJL, 787, L30
Reines, A. E., Reynolds, M. T., Miller, J. M., et al. 2016, ApJL, 830, L35
Reines, A. E., & Volonteri, M. 2015, ApJ, 813, 82
Stierwalt, S., Besla, G., Patton, D., et al. 2015, ApJ, 805, 2
Treister, E., Schawinski, K., Urry, C. M., & Simmons, B. D. 2012, ApJL, 758, L39
Vaughan, S., Iwasawa, K., Fabian, A. C., & Hayashida, K. 2005, MNRAS, 356, 524
Volonteri, M. 2010, A&ARv, 18, 279
Volonteri, M., Habouzit, M., & Colpi, M. 2021, NatRP, 3, 732
Zou, F., Brandt, W. N., Ni, Q., et al. 2023, ApJ, 950, 136